A new process-based and scale-aware desert dust emission scheme for global climate models – Part II: evaluation in the Community Earth System Model (CESM2)

Danny M. Leung[1], Jasper F. Kok[1], Longlei Li[2], Natalie M. Mahowald[2], David M. Lawrence[3], Simone Tilmes[3], Erik Kluzek[3], Martina Klose[4], Carlos Pérez García-Pando[5,6]

[1]Department of Atmospheric and Oceanic Sciences, University of California – Los Angeles, Los Angeles, California, USA
[2]Department of Earth and Atmospheric Sciences, Cornell University, Ithaca, New York, USA
[3]National Center for Atmospheric Research, Boulder, Colorado, USA
[4]Institute of Meteorology and Climate Research (IMK-TRO), Department Troposphere Research, Karlsruhe Institute of Technology (KIT), Karlsruhe, Germany
[5]Barcelona Supercomputing Center (BSC), Barcelona, Spain
[6]Catalan Institution for Research and Advanced Studies (ICREA), Barcelona, Spain

Correspondence to: Danny M. Leung (dannymleung@ucla.edu)

Section S1. Significance in correlation differences.

For Fig. 10f, we use Fisher's Z transformation (Fisher, 1992) to test how significant a Pearson correlation coefficient is different from another. To compute a 2-tailed p-value of difference in correlations, the computation is a function of the two correlations (e.g., MIDAS DAOD vs. our scheme's DAOD as R_1; MIDAS DAOD vs. Z03's DAOD as R_2) and the sample size (for each grid, 2004–2008 daily data are in total $n_1 = n_2 = 1827$):

$$Z_1 = 0.5\ln\left(\frac{1+R_1}{1-R_1}\right) \quad \text{(S1)}$$

$$Z_2 = 0.5\ln\left(\frac{1+R_2}{1-R_2}\right) \quad \text{(S2)}$$

$$\text{score} = \frac{Z_1 - Z_2}{\sqrt{\frac{1}{n_1 - 3} + \frac{1}{n_2 - 3}}} \quad \text{(S3)}$$

Then we use the look up table to yield the p-value for the score. For computers,

$$p \text{ value} = 2 \times \text{pnorm}(\text{abs}(\text{score})) \quad \text{(S4)}$$

Then, for instance,

If $R_1 = 0.45, R_2 = 0.4$, then p-value ~ 0.065 > 0.05;
If $R_1 = 0.65, R_2 = 0.6$, then p-value ~ 0.013 < 0.05;
If $R_1 = 0.85, R_2 = 0.8$, then p-value ~ 10^{-6} << 0.05.

Comparing with other maps of correlation differences in Figs. 6d-f with $|\Delta R|$ of 0.1–0.3, Fig. 10f overall has grids with much smaller $|\Delta R|$ values of < 0.02, which are not statistically significant. $|\Delta R|$ for any gridcell has to be > 0.082 to yield a p-value of < 0.05.

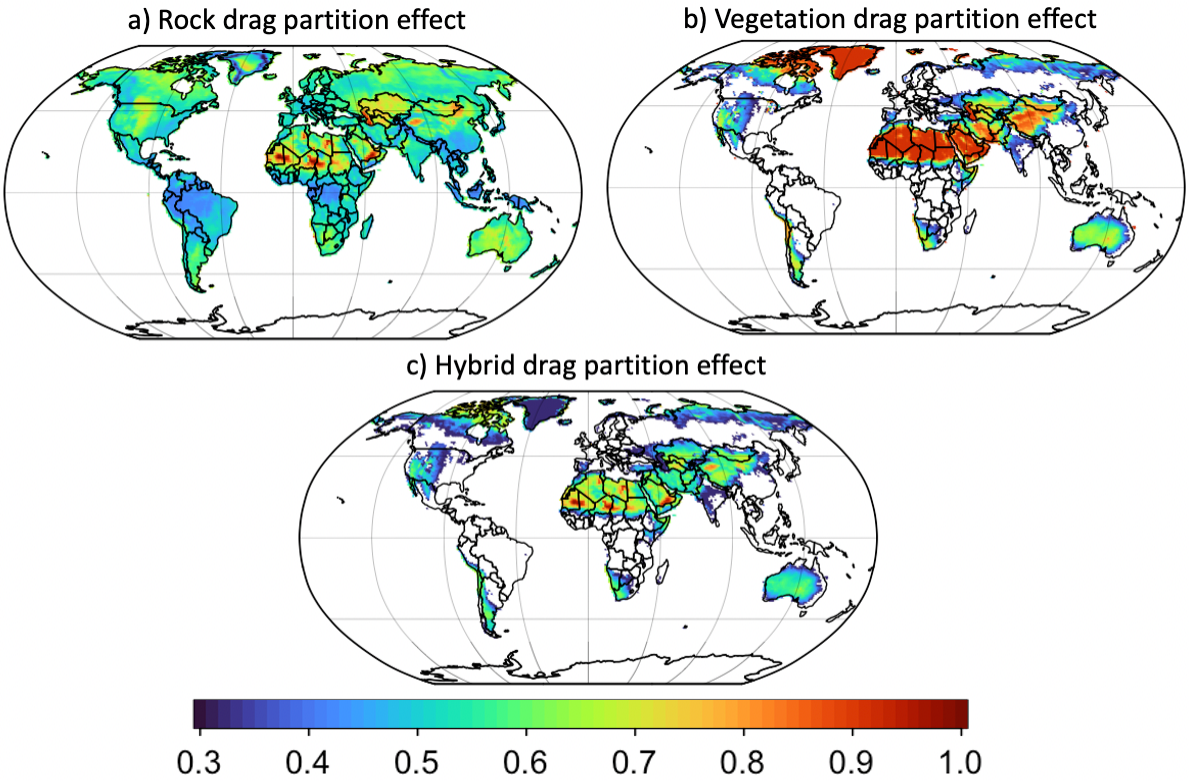

Figure S1. Drag partition effects due to (a) rocks, (b) green + brown vegetation, and (c) their combined effect.

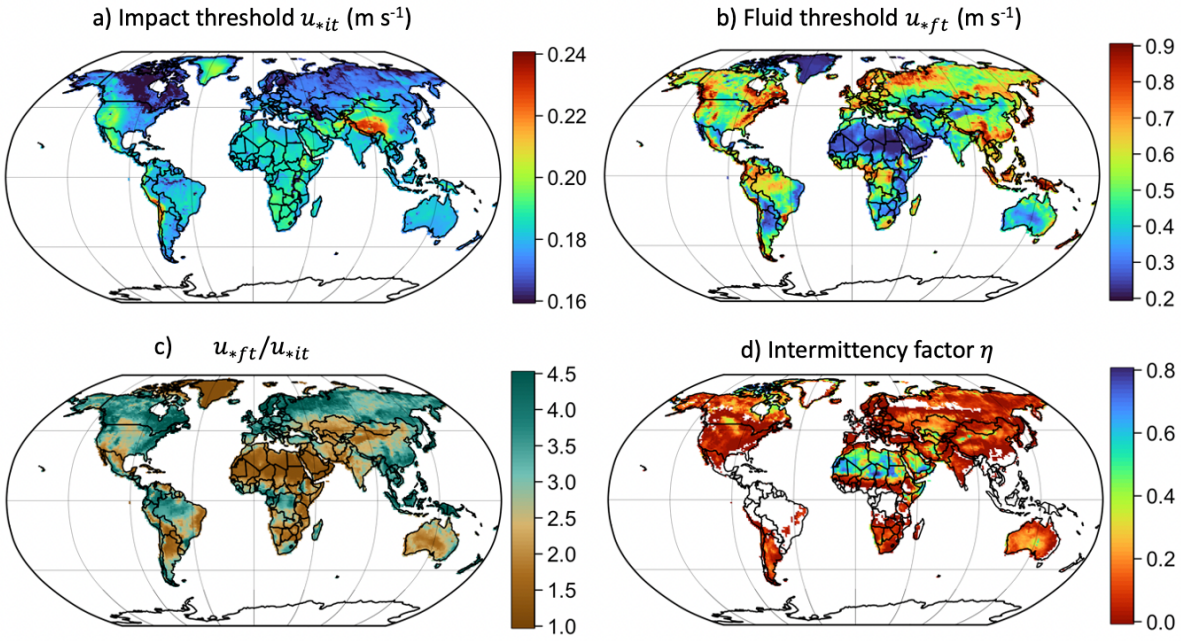

Figure S2. Dust emission thresholds and intermittency factor simulated by CLM5. (a) impact threshold friction velocity u_{*it}, (b) fluid threshold friction velocity u_{*ft}, (c) ratio of fluid to impact threshold u_{*ft}/u_{*it}, and (d) intermittency factor η for 2004–2008.

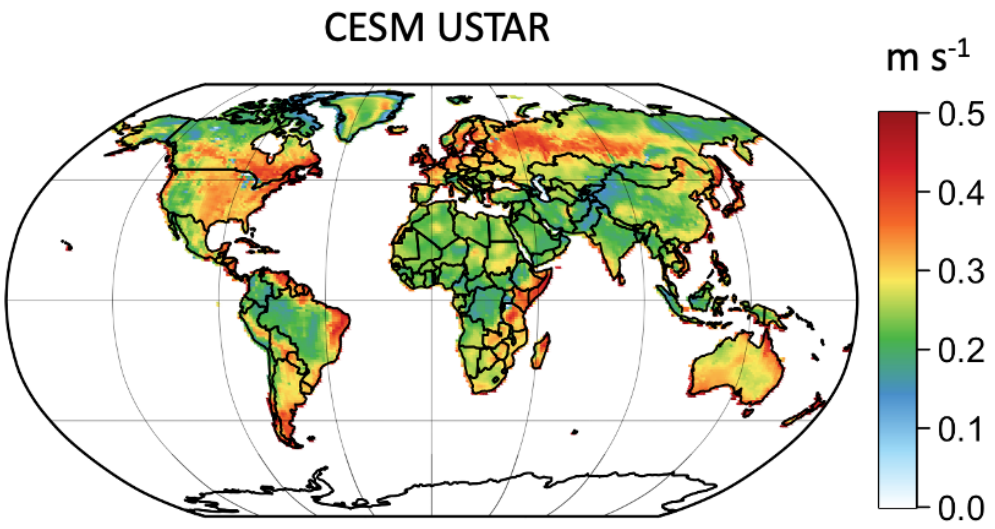

Figure S3. The CESM2 2004–2008 mean friction velocity u_* (m s^{-1}) for calculating dust emissions in CLM5. The wind comes from CAM6 with its meteorology nudged toward the MERRA-2 meteorology.

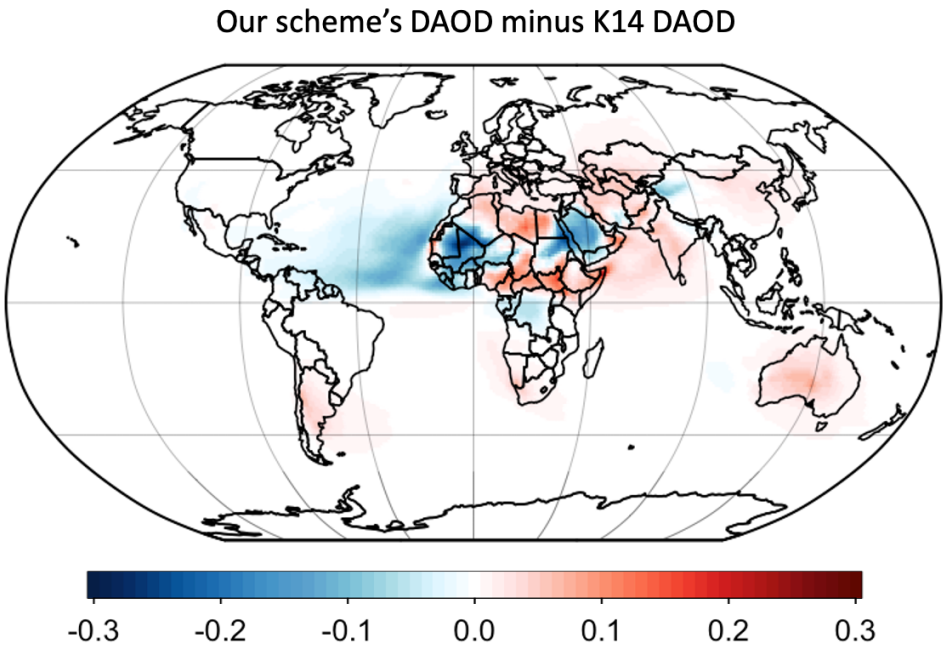

Figure S4. Global DAOD difference between our new scheme (Leung et al., 2022) and the K14 scheme, i.e., Fig. 3b minus Fig. 3a.

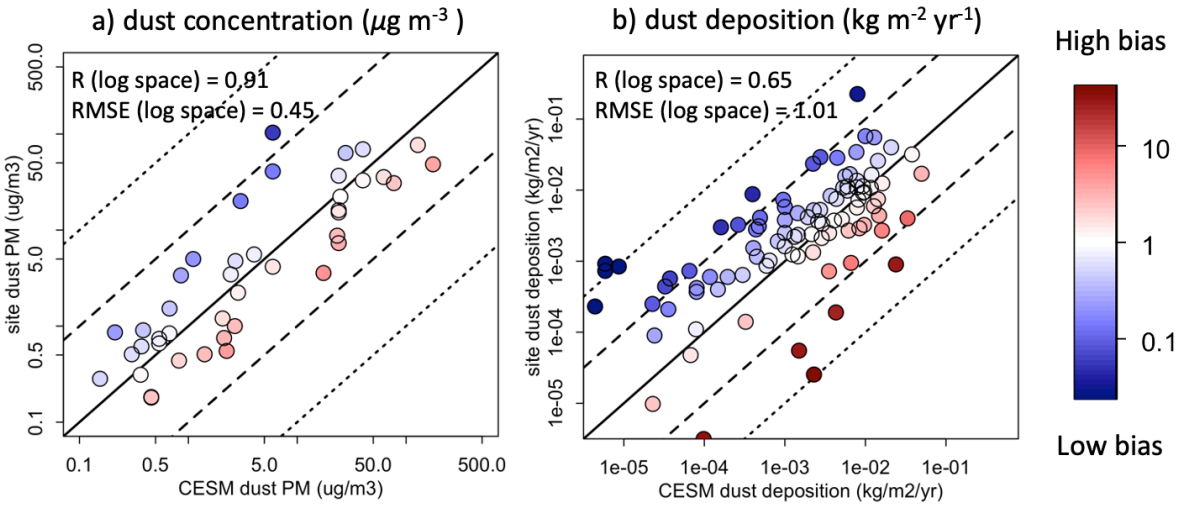

Figure S5. Our scheme's dust PM concentrations (in μg m^{-3}) and depositions (in kg m^{-2} yr^{-1}) after implementing the scaling map $\widetilde{K}_c$, versus site dust PM concentrations and depositions.

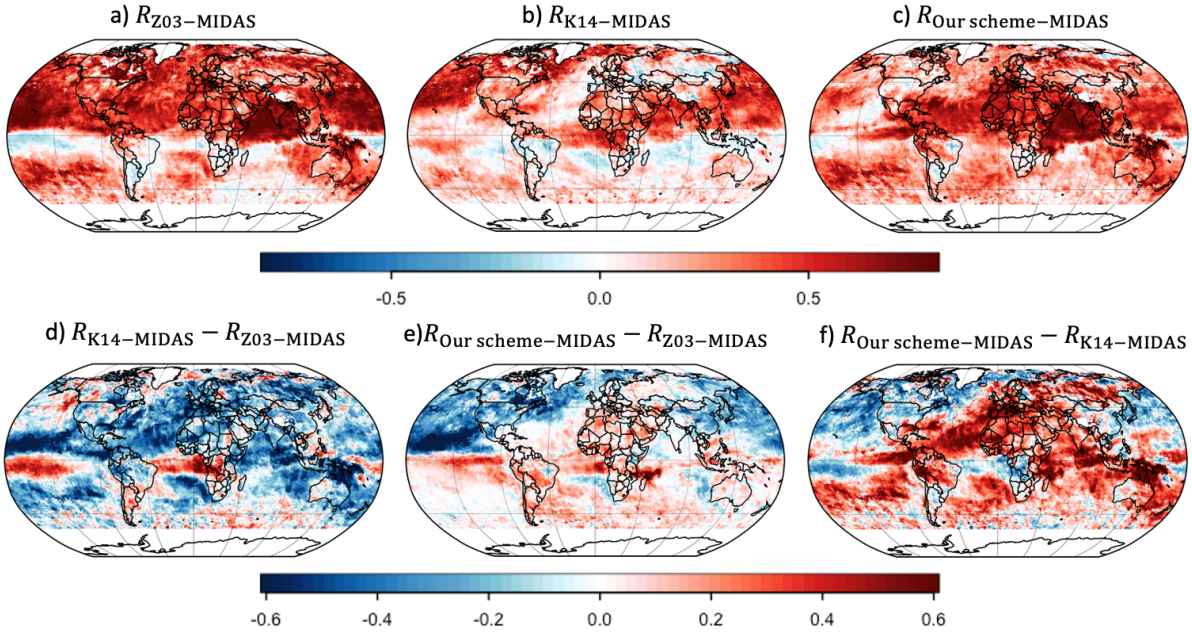

Figure S6. Grid-by-grid MIDAS DAOD daily correlation maps with CESM2 for 2004–2008. (a-c) Correlation maps R of MIDAS daily DAOD time series vs. CESM2 daily DAOD time series using (a) Z03, (b) K14, and (c) our scheme. The correlation maps focus on gridboxes with MIDAS DAOD/AOD ratio > 0.25 only. (d–f) Changes (ΔR) in correlation maps between CESM and MIDAS DAOD, from (d) Z03 to K14, (e) Z03 to our scheme, and from (f) K14 to our scheme. This figure is the same as Fig. 6 in the main text but no masking for low MIDAS DAOD / AOD values.

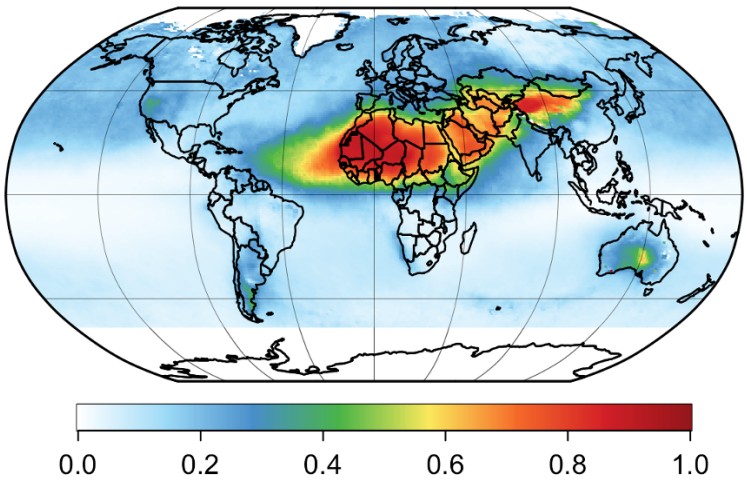

Figure S7. MIDAS DAOD / AOD values averaged across 2004–2008. Polar regions and snow/ice covered continents have no values (white color).

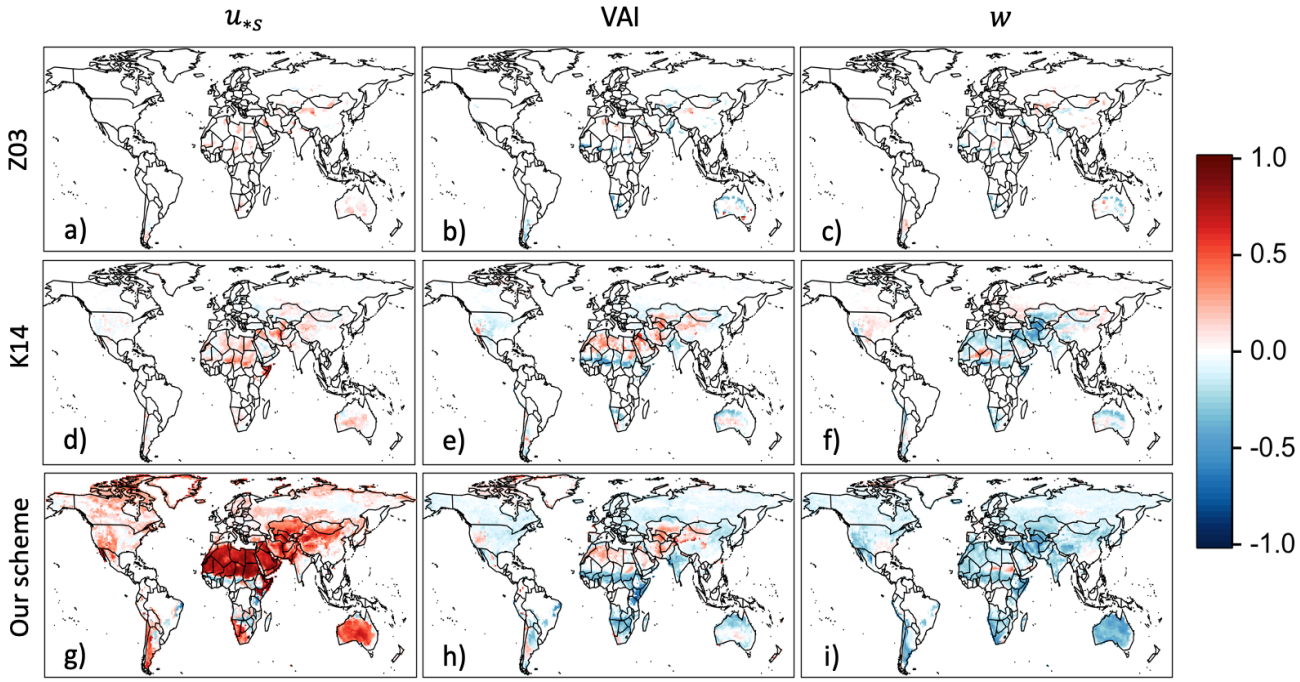

Figure S8. Grid-by-grid daily Pearson correlation maps between simulated dust emissions and the three fundamental driving meteorological fields in CESM2 for 2004–2008. Each row represents an emission scheme, including (a-c) Z03, (d-f) K14, and (g-i) our scheme. Each column represents a meteorological or land surface field in CESM2 that fundamentally drives dust emission, including soil surface friction velocity u_{*s} (m s^{-1}) as the left column (we use u_* for Z03 and K14), vegetation area index (VAI; m^2 plant / m^2 land) as the middle column, and soil moisture w (kg water / kg soil) as the right column.

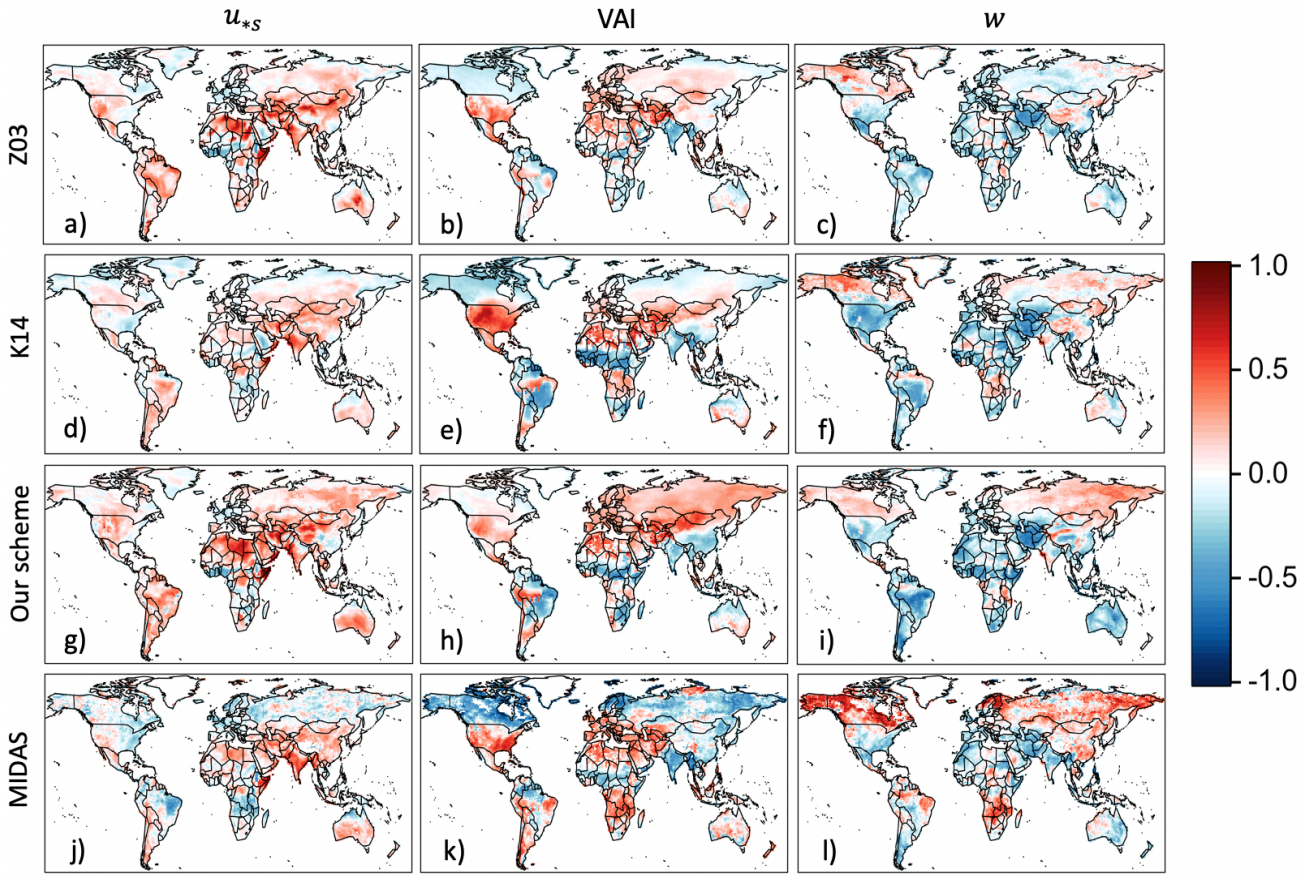

Figure S9. Grid-by-grid daily Pearson correlation maps between DAOD and the three fundamental driving meteorological fields in CESM2 for 2004–2008. The first three rows use the DAOD simulated using different emission schemes in CESM2, respectively (a-c) Z03, (d-f) K14, and (g-i) our scheme, and the last row uses MIDAS DAOD. Each column represents a meteorological or land surface field in CESM2 that fundamentally drives dust emission, including soil surface friction velocity u_{*s} (m s^{-1}) as the left column (we use u_* for Z03 and K14, and MIDAS), vegetation area index (VAI; m^2 plant / m^2 land) as the middle column, and soil moisture w (kg water / kg soil) as the right column. Note that the DAOD correlations do not cover the oceans because the meteorological and land surface fields used here are only defined over the continents.

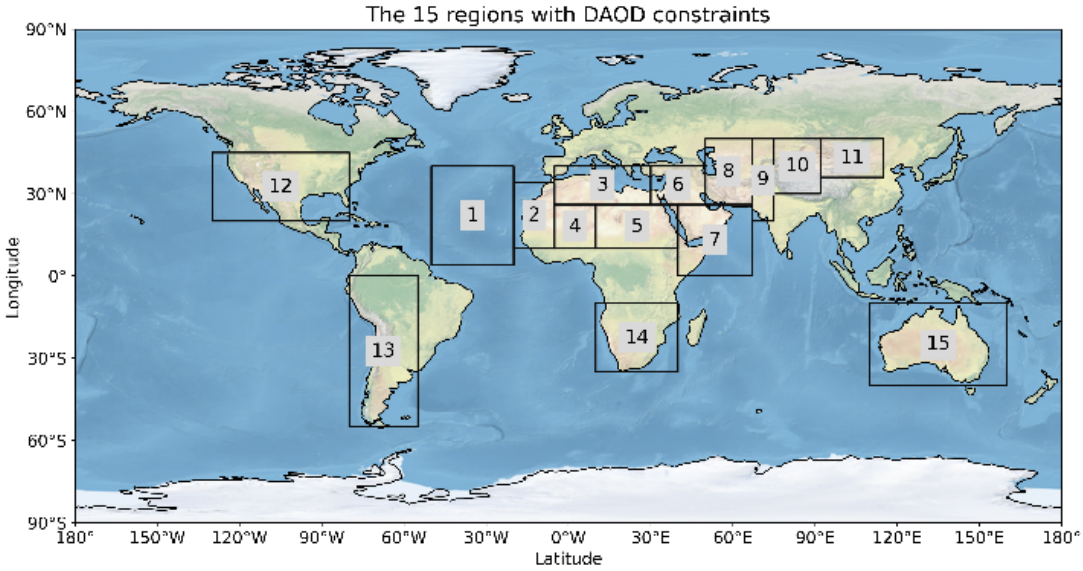

Figure S10. Coordinates of the 15 observed dusty regions with the Ridley et al. (2016) constraints on the regional DAOD. The coordinates of the 15 dusty regions are: (1) Mid-Atlantic (50–20°W; 4–40°N), (2) African west coast (20–5°W; 10–34°N), (3) Northern Africa (5°W–30°E; 26–40°N), (4) Mali / Niger (5°W–10°E; 10–26°N), (5) Bodélé / Sudan (10–40°E; 10–26°N), (6) Northern Middle East (30–50°E; 26–40°N), (7) Southern Middle East (40–67.5°E; 0–26°N), (8) Kyzylkum (50–67.5°E; 26–50°N), (9) Thar (67.5–75°E; 20–50°N), (10) Taklamakan (75–92.5°E; 30–50°N), (11) Gobi (92.5–115°E; 36–50°N), (12) North America (130–80°W; 20–45°N), (13) South America (80–55°W; 55–0°S), (14) Southern Africa (10–40°E; 35–10°S), and (15) Australia (110–160°E; 40–10°S). The figure is adapted from Kok et al. (2021).